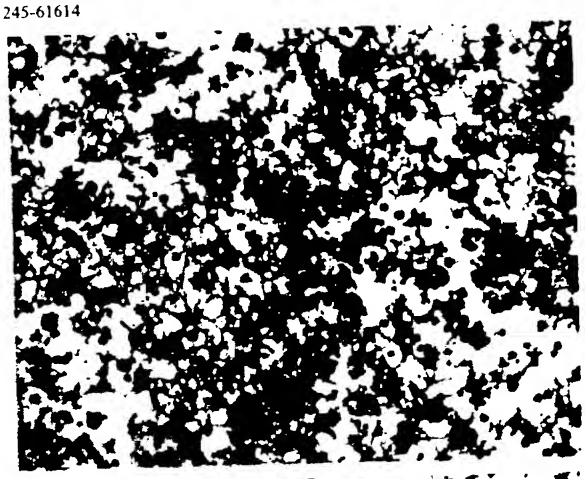

FIG. 1A

Top: No treatment

Bottom: Norepinephrine

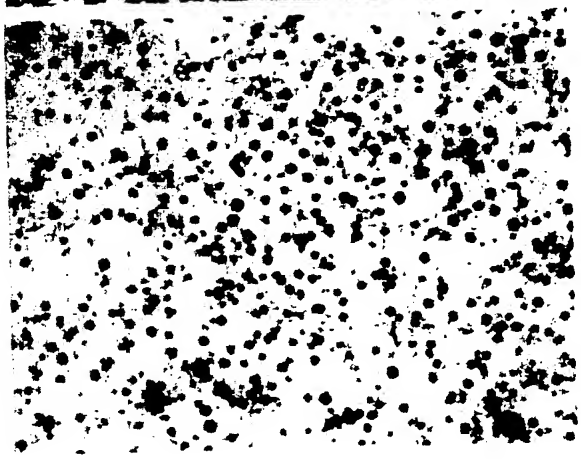

FIG. 1B

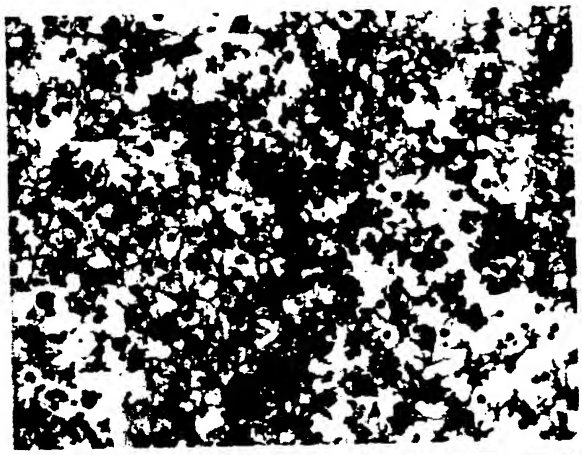

FIG. 2A

Top: No treatment

Bottom: Cholera toxin

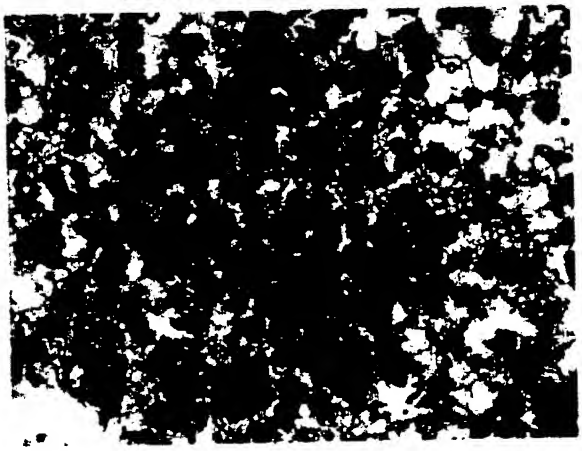

FIG. 2B

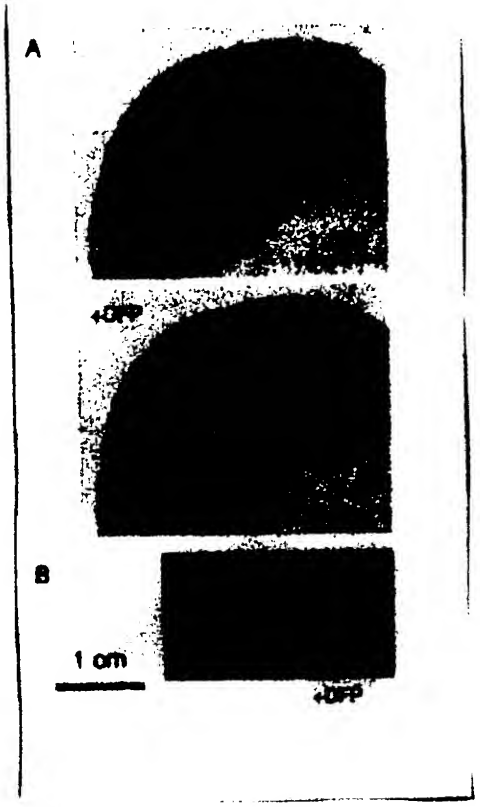

FIG. 3A

FIG. 3B

FIG. 3C

FIG. 4A

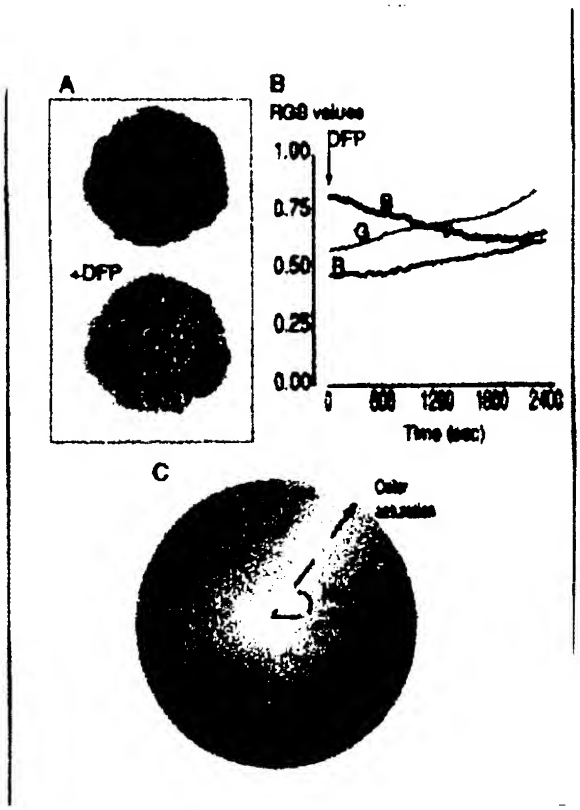

FIG. 4B

FIG. 4C

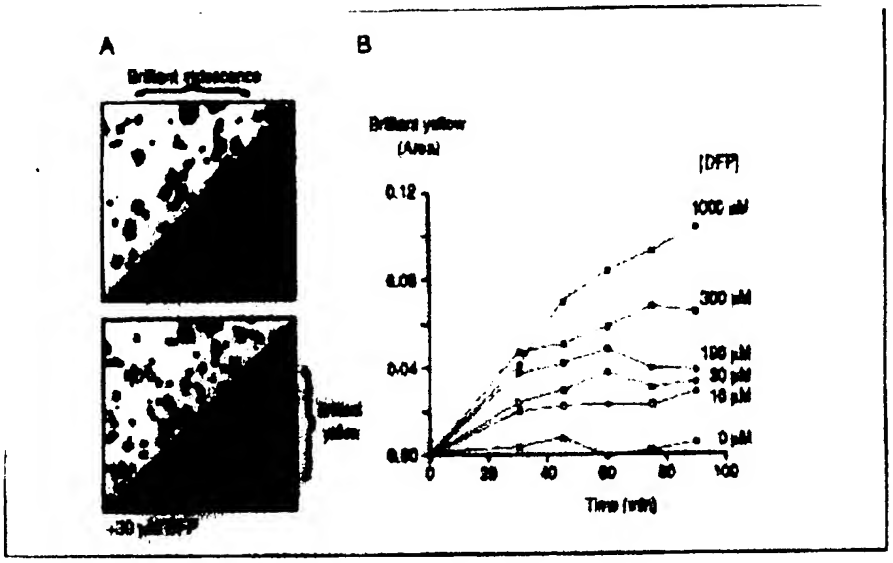

FIG. 5A

FIG. 5B

FIG. 6A

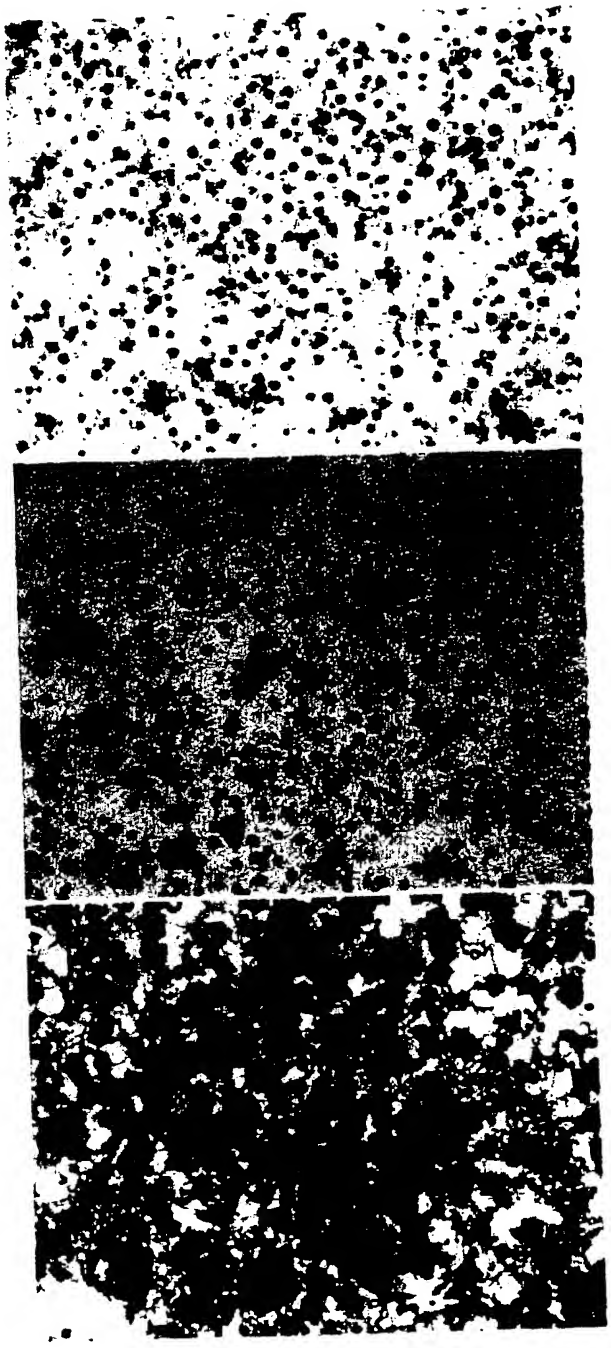

Top: No pre-incubation with cholera toxin, followed by norepinephrine

Middle: Pre-incubation with a threshold dose of cholera toxin, followed by norepinephrine

FIG. 6B

Bottom: Pre-incubation with a higher dose of cholera toxin, followed by norepinephrine.

FIG. 6C

Before adding bacteria After adding bacteria

Strain 1

FIG. 7A

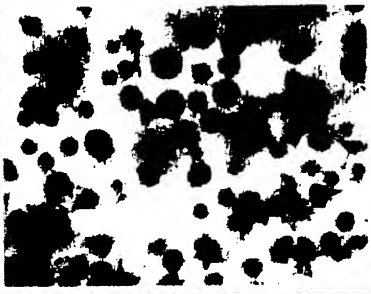

FIG. 7B

Strain 2

FIG. 8A

FIG. 8B

Strain 3

FIG. 9A

FIG. 9B

Strain 4

FIG. 10A

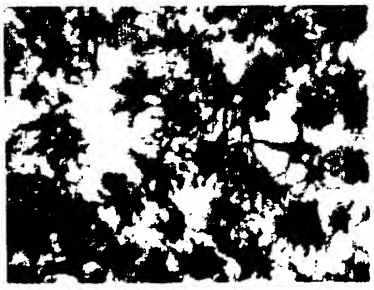

FIG. 10B

Strain 5

FIG. 11A

FIG. 11B

This is an example of a before (top)-and-after (bottom) shot of the effects of bacteria on cultured chromatophores.

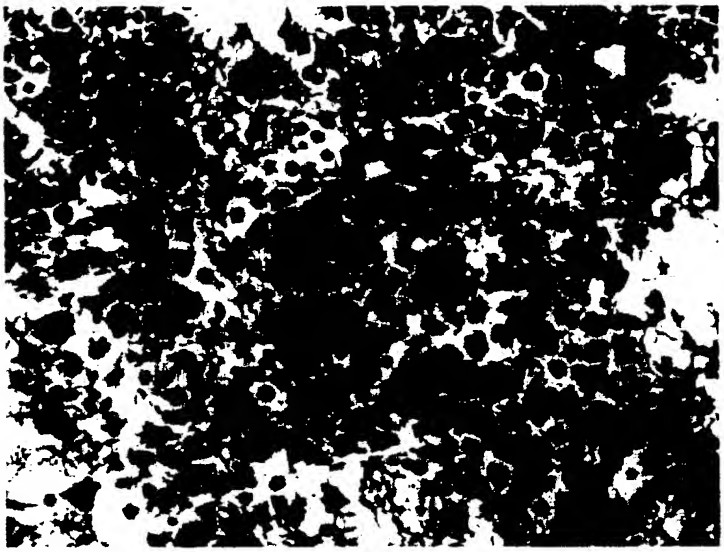

FIG. 12A

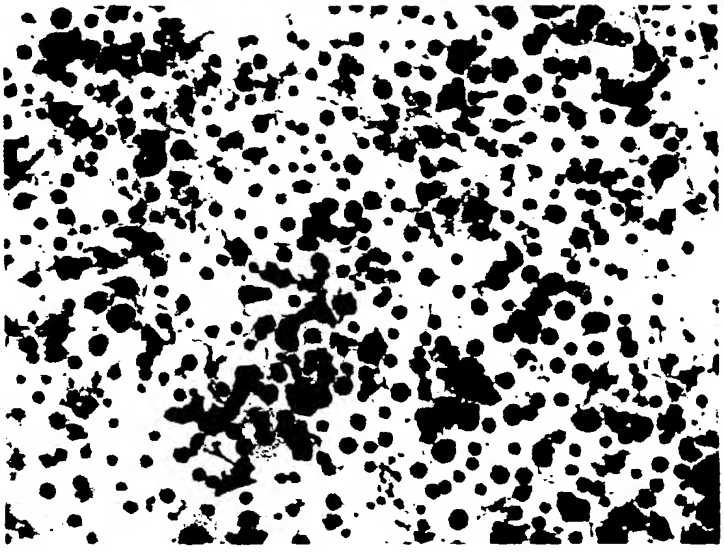

FIG. 12B

	Agent	Chemical Type	Effective dose	Direct Effects	Challenge A (norepinephrine)	Challenge B (forskolin)
Control	None					
I	DFP Mipafox Paraoxon	phosphorofluoridate phosphorofluoroamidate phosphate	ppm			
II	PMSF EPN	sulfonylfluoride phosphonothioate	ppm			
III	Mevinphos Dichlorvos	phosphate phosphate	ppt			
IV	Trichlorfon	phosphonate	ppt			
V	Chlorpyrifos Fenitrothion Merphos Carbaryl Methomyl 2,5 Hexanedione Acrylamide	phosphorothioate phosphorothioate phosphorotrithioate carbamate carbamate diketone amide	ND			

FIG. 13

The appearance of chromatophore **sensor cells** varies according to their exposure to bioactive agents, as illustrated by these high-magnification examples.

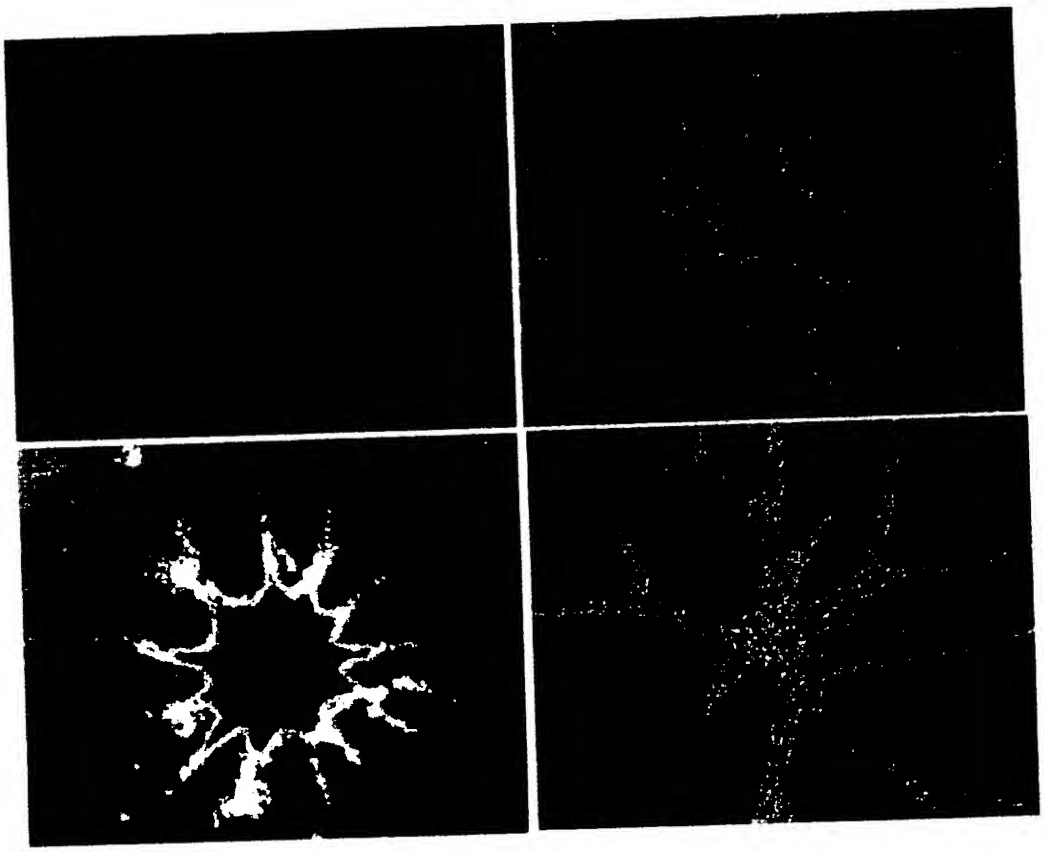

FIG. 14A

FIG. 14B

FIG. 14C

FIG. 14D

Figure 1. Species-comparison of chromatophore plating density and morphology. Top, Betta splendens chromatophores cultured on polystyrene. Bottom, Hemichromis bimaculatus chromatophores, cultured on polystyrene by identical methods. The same size bar applies to both images.

FIG. 15A

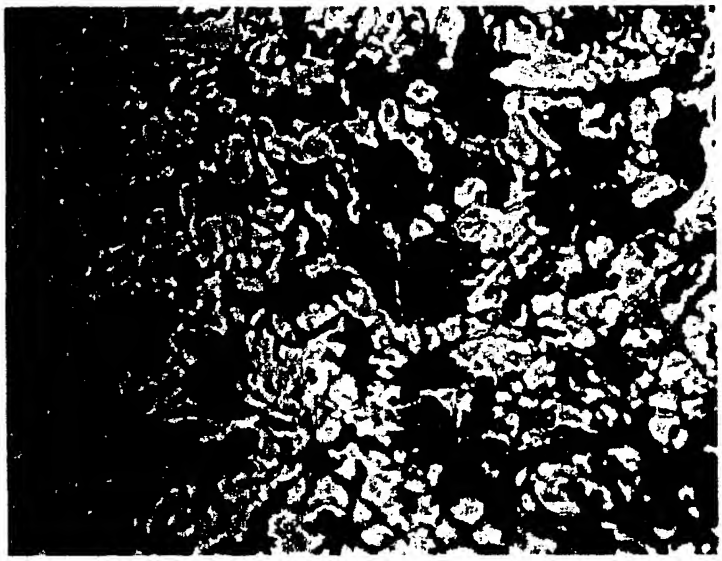

FIG. 15B

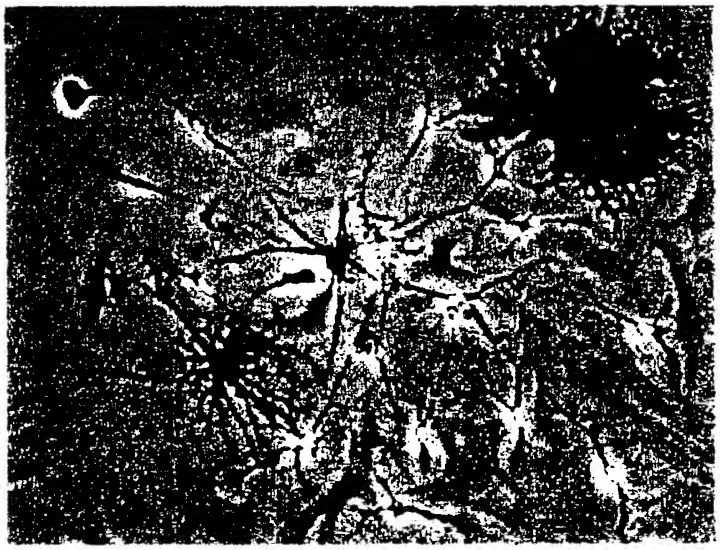

100 microns

Scales from three color variants of Betta splendens. These are basal colors, with no biologically active agent added.

FIG. 16A FIG. 16B FIG. 16C

The cultured chromatophores from a Violet variant of Betta splendens were photographed with a dark-field background, a lighting technique which accentuates both the pigmented erythrophores and the blue-hued iridophores. This field of view shows the basal appearance of the cells, with no added biologically active agents.

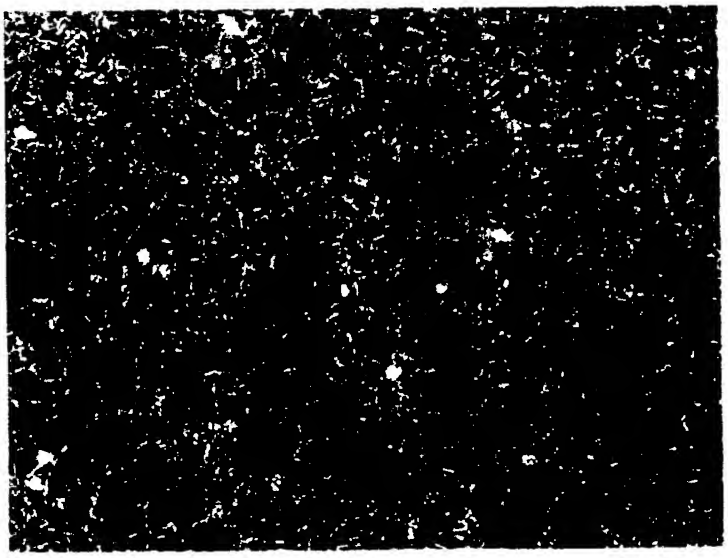

FIG. 17

Hardware construction for the encapsulation of SOS sensor cells.

FIG. 18A

Extruder hardware (assembled)

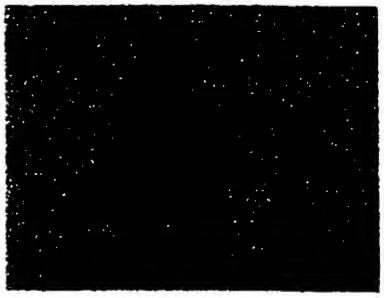

FIG. 18B

FIG. 18C

Air-flow adjustment mechanism

FIG. 19A

(+) Ca^{2+}

FIG. 20A

(-) Ca^{2+}

Before

After 10nM Norepinephrine

FIG. 19B

FIG. 20B

Figure 1: Demonstration of the dependence of Ca^{2+} on pigment aggregation in erythrophores. (+) Ca^{2+} (first column): Performed in media containing 1.8 mM added Ca^{2+}. (-) Ca^{2+} (second column): Performed in media with no added Ca^{2+} plus 1mM EGTA. Before images were captured immediately prior to norepinephrine exposure and after images were captured 10 minutes after exposure.

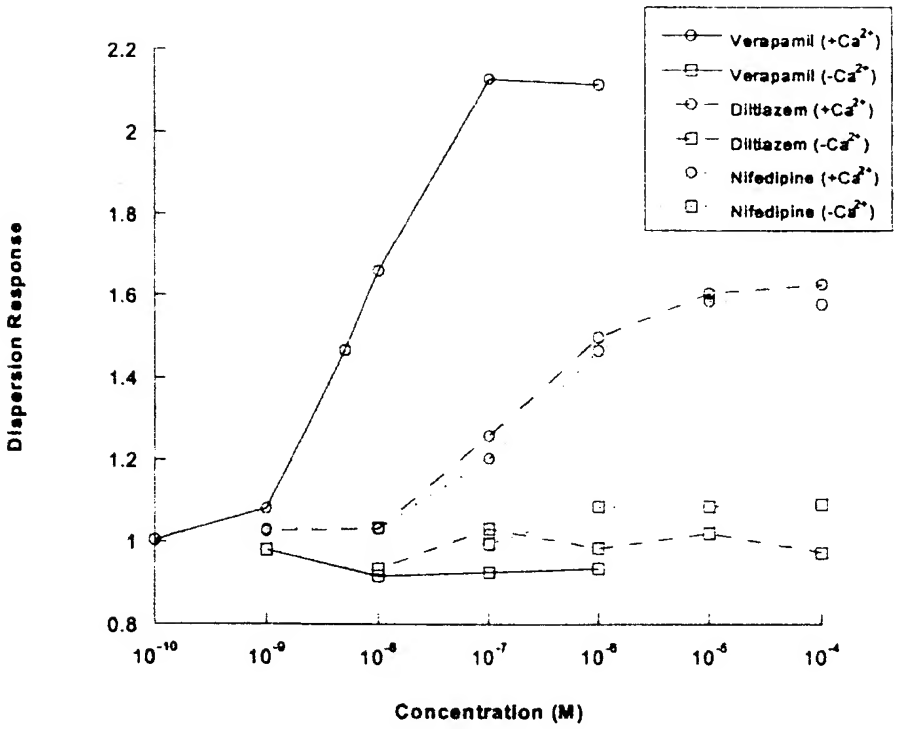

Figure 2: Erythrophore dose responses to L-type Ca^{2+} channel blockers verapamil, nifedipine, and diltiazem. Erythrophores were treated at each data point with 1nM norepinephrine for at least 5 minutes prior to exposure of the channel blockers. The dispersion response was calculated as area occupied by the cells after chemical exposure for 10 minutes divided by the area occupied before exposure. (+) Ca^{2+} experiments were performed in PSS containing 1.8mM added Ca^{2+}. (–) Ca^{2+} experiments were performed in PSS with no added Ca^{2+} plus 1mM EGTA to demonstrate the requirement of extracellular Ca^{2+} for channel blockers to block inward movement of Ca^{2+} and thus cause direct dispersion of erythrophores.

FIG. 21

FIG. 21

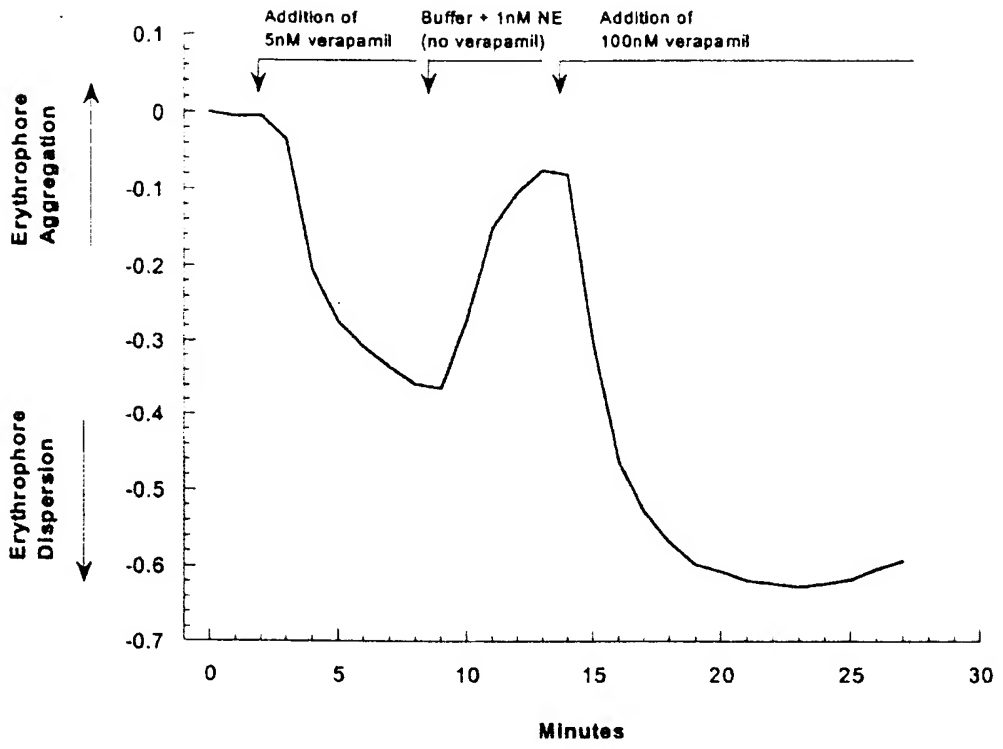

FIG. 22

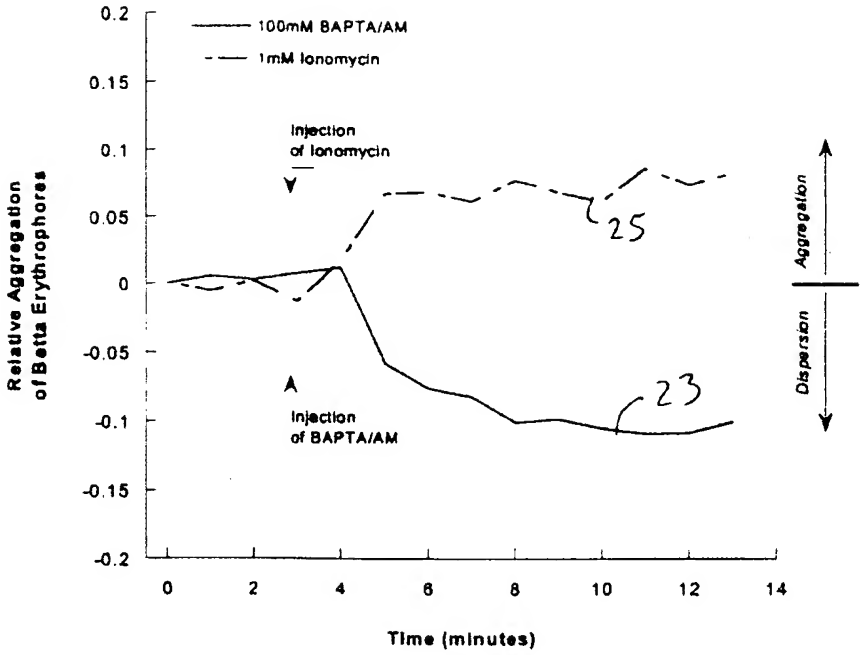

FIG. 23

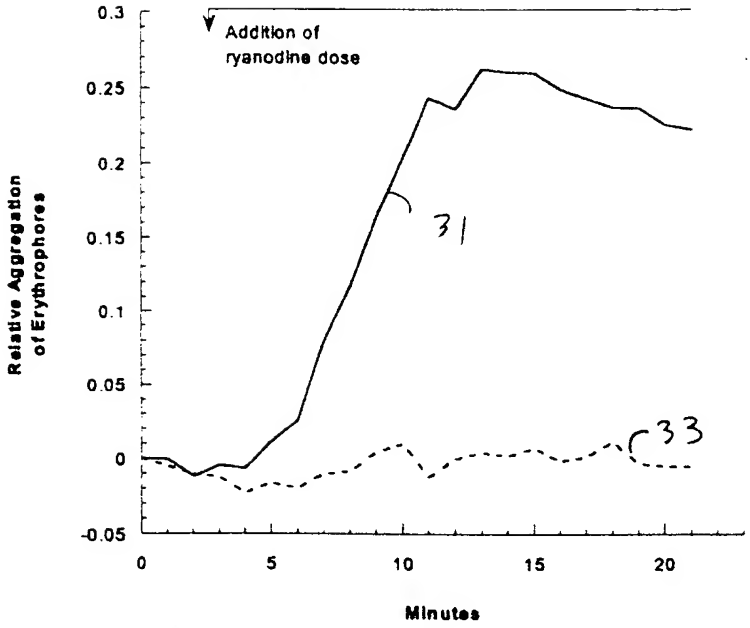

Aggregation response in Betta erythrophores from ryanodine exposure at 10nM (solid line) and 10μM (dashed line) – Ryanodine doses in PSS were added at the time point indicated and allowed to incubate with erythrophores for the remainder of the experiment. Recent literature has indicated that ryanodine at doses <1μM are effective at stimulating Ca^{2+} release from the endoplasmic reticulum via ryanodine receptors; however, doses >1μM inhibit Ca^{2+} release through the same receptors. This data is consistent with these reports. The delay in initial erythrophore response after dose addition may be the result of the time required for the molecule to pass through the plasma membrane and reach its intracellular target.

FIG. 24

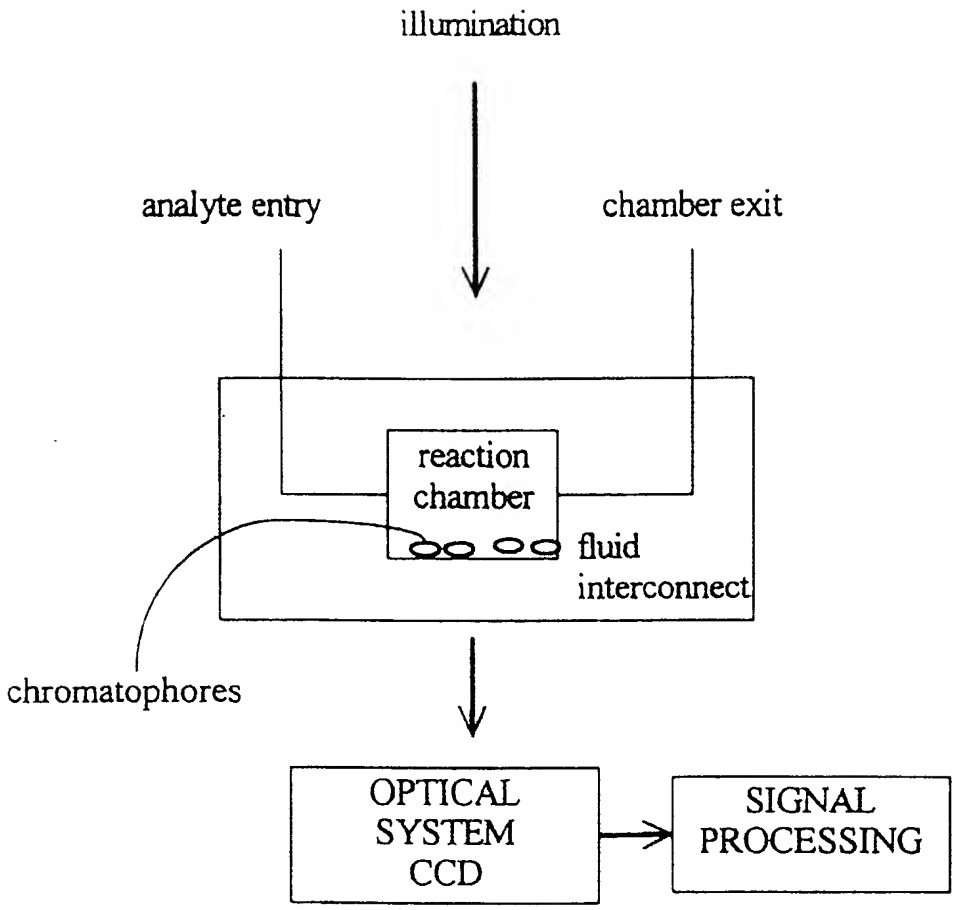

FIG. 25

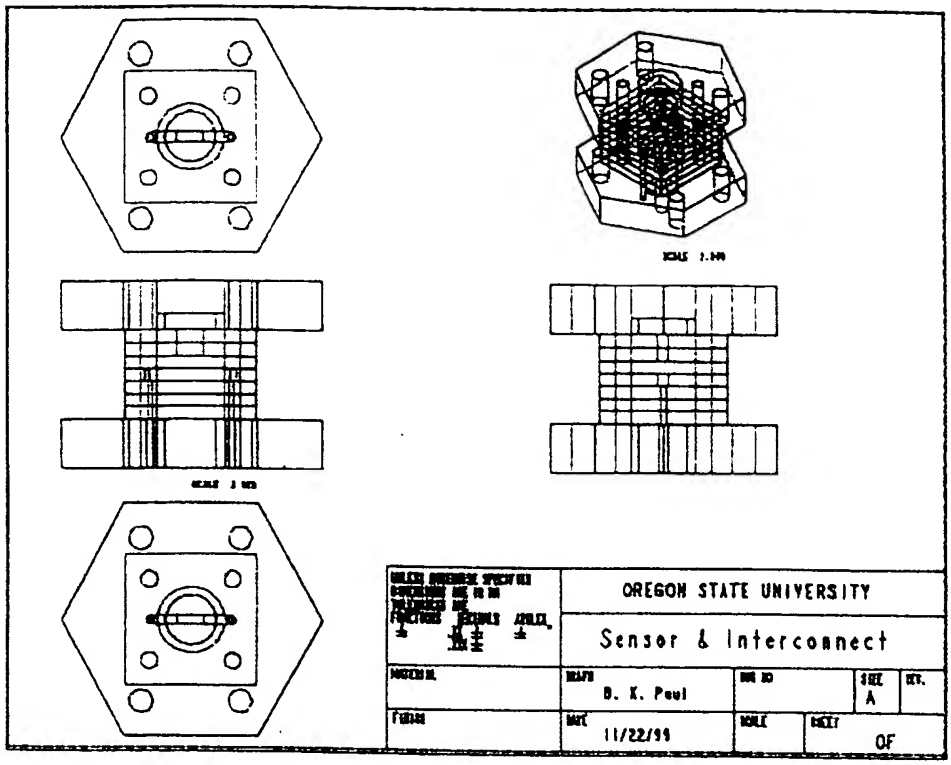

FIG. 26A

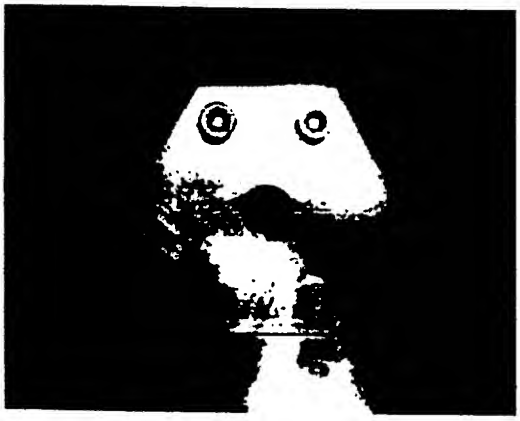

FIG. 26B

Engineering diagram and photograph of a cell chamber sandwiched within the fluidic interconnect. In the engineering diagram the thickness of the cell chamber has been exaggerated for clarity.

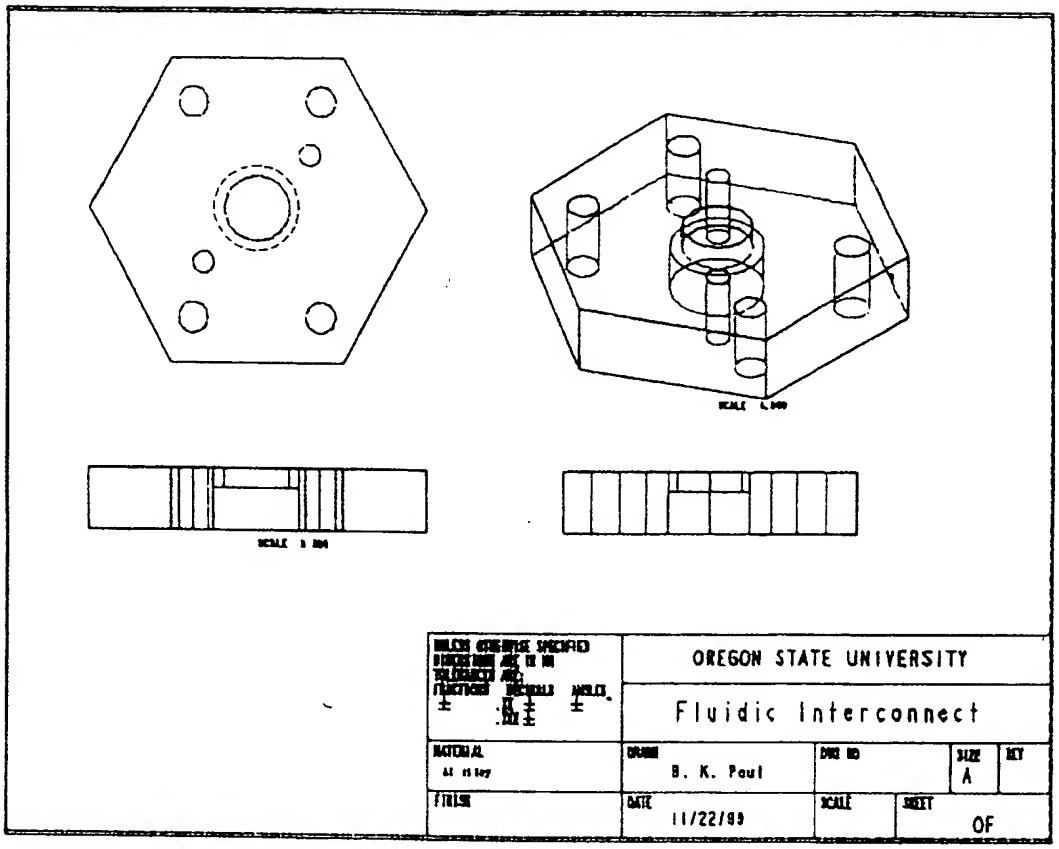

Engineering diagram showing one side of the fluidic interconnect.

FIG. 27

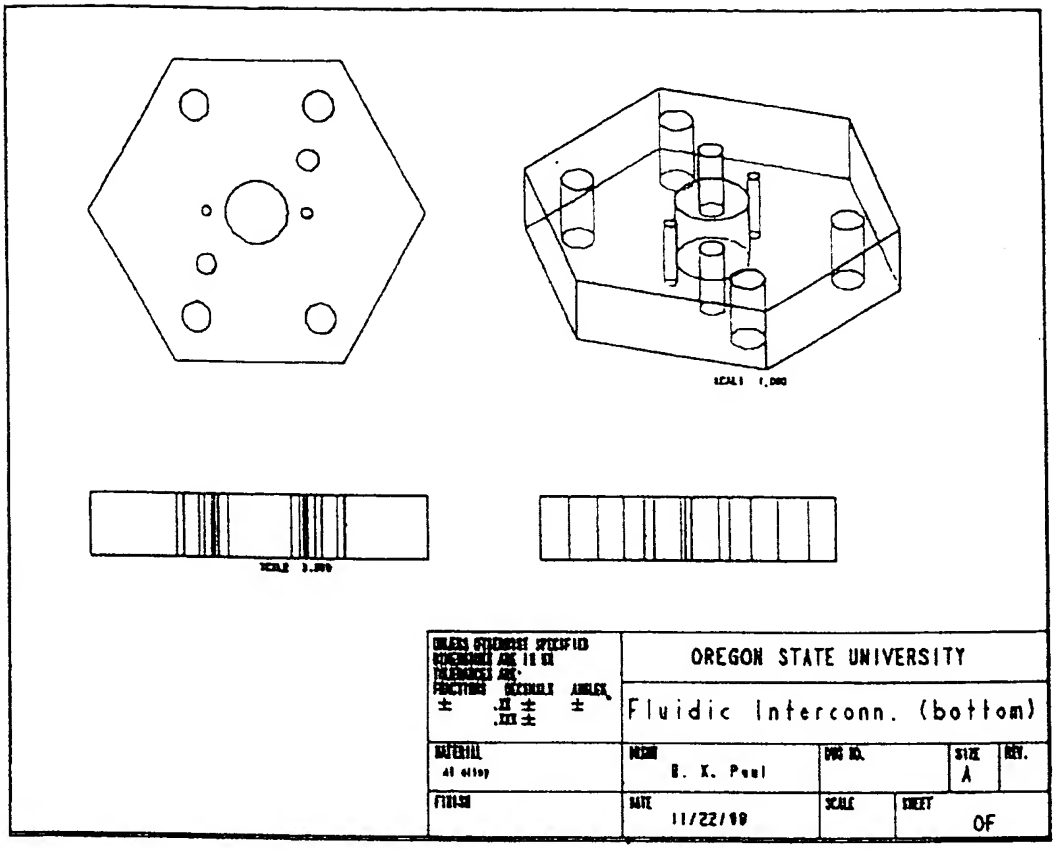

FIG. 28A

FIG. 28B

Engineering diagram showing the other side of the fluidic interconnect. The photograph shows both sides of the fluidic interconnect. Mounted on the left side of the interconnect is a transparent version of a cell chamber.

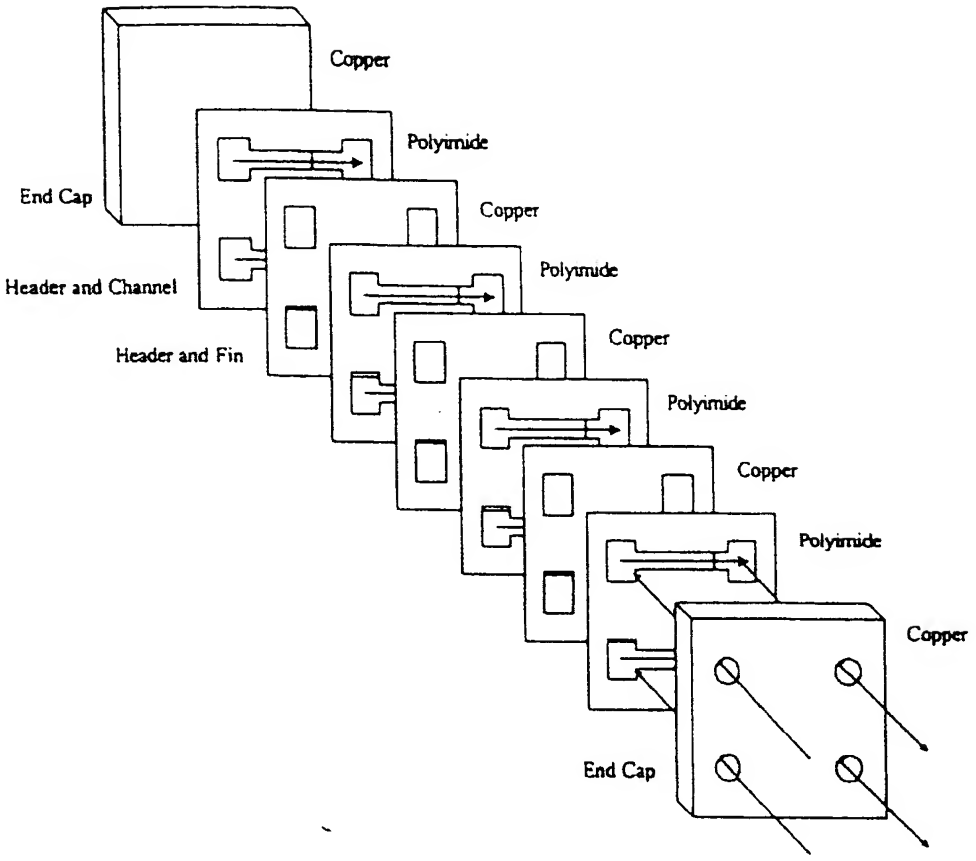

Microlamination sheme used to fabricate a dual microchannel array. Arrows show direction of flow. In this case, laminae are bonded by use of the polyimide as a thermal adhesive.

FIG. 29

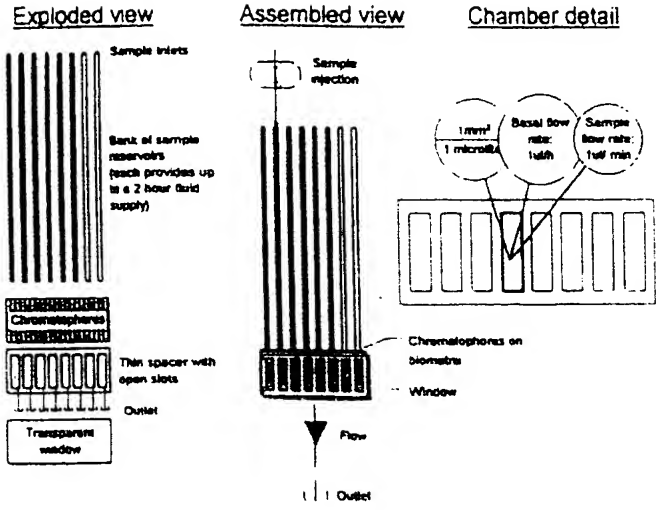

FIG. 30A FIG. 30B FIG. 30C

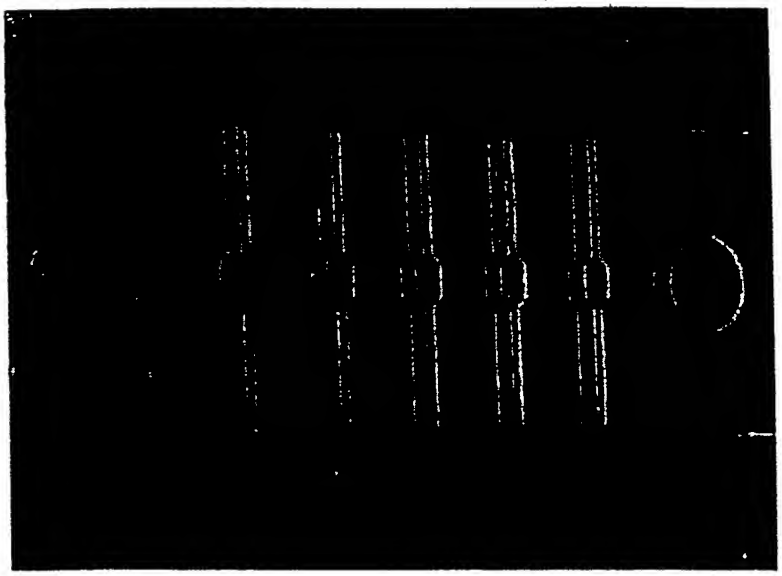

FIG. 31

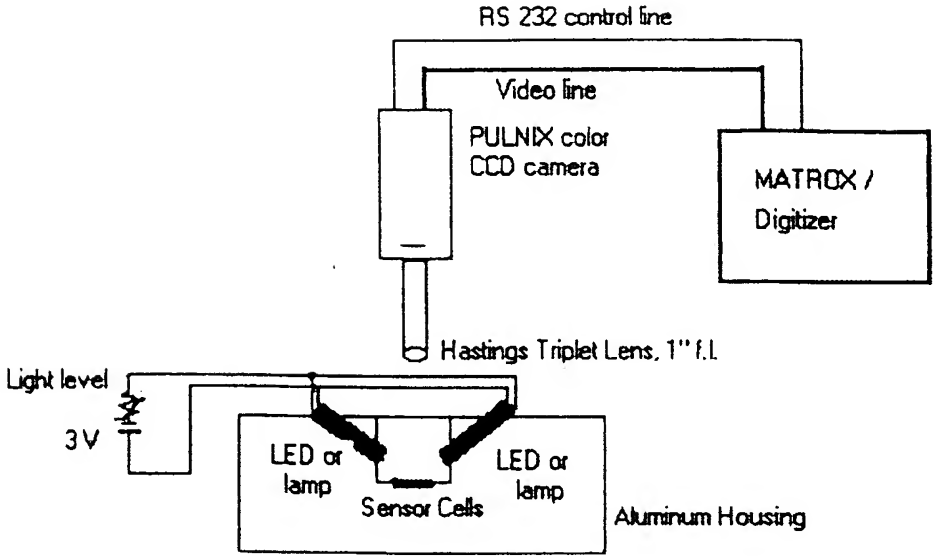

FIG. 32

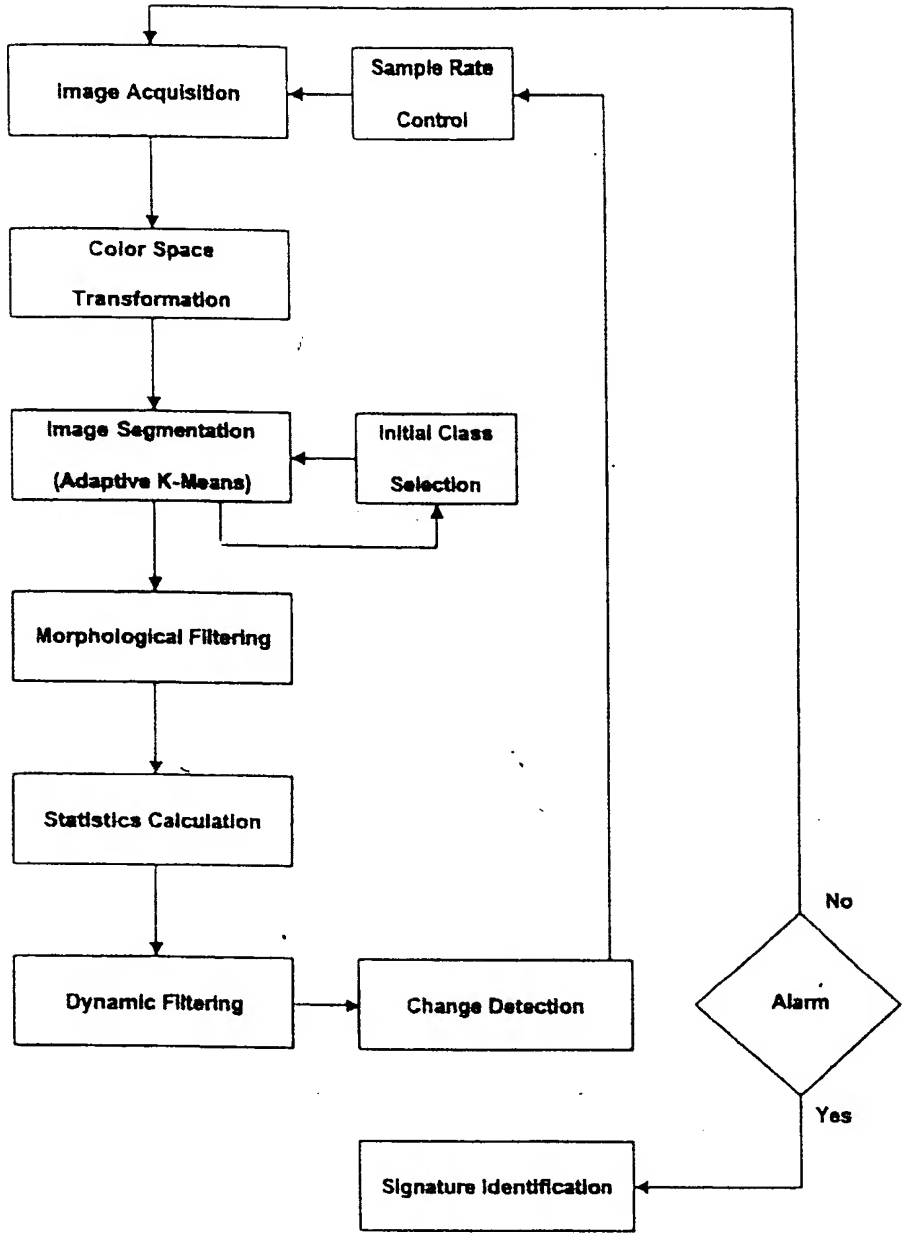

FIG. 33

A screen shot showing the output from the analyzer. The x-axis represents time (frame number). The y-axis represents an abstract count of cell color and morphology. The curve is essentially an indicator of the optical status of the sensor cells, and the dip in the plot occurring at frame 58 shows that the optical status changed. Indeed, norepinephrine had been injected into the cytosensor a few frames earlier. However, an x-y plot like this does not in itself provide a judgment call based on statistical probabilities. The algorithm therefore makes additional statistical calculations and reports those as the horizontal bar immediately above the x-y plot. That bar is colored green, except for a period of about 10 frames when it is colored red (from frame 58 to 68). The red color symbolizes the rejection of the null hypothesis, i.e. red means there was a greater than 99% probability that the sensor cells had changed their optical appearance. Thus, a judgment call has been made by the algorithm, and the red portion of the bar can be viewed as a positive alarm signal.

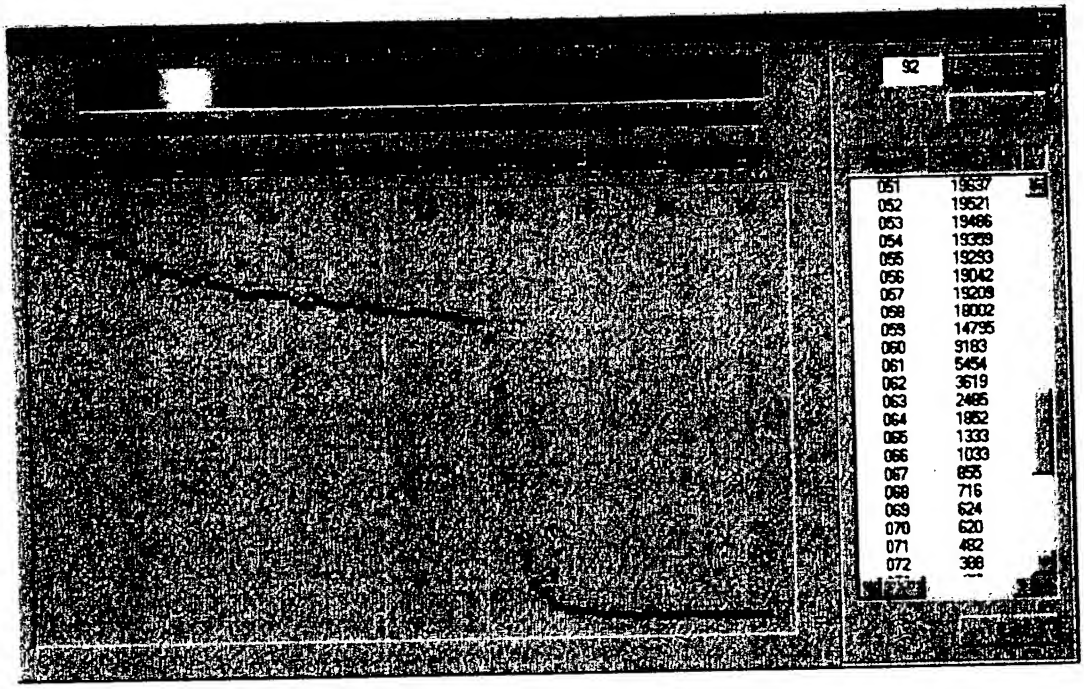

FIG. 34

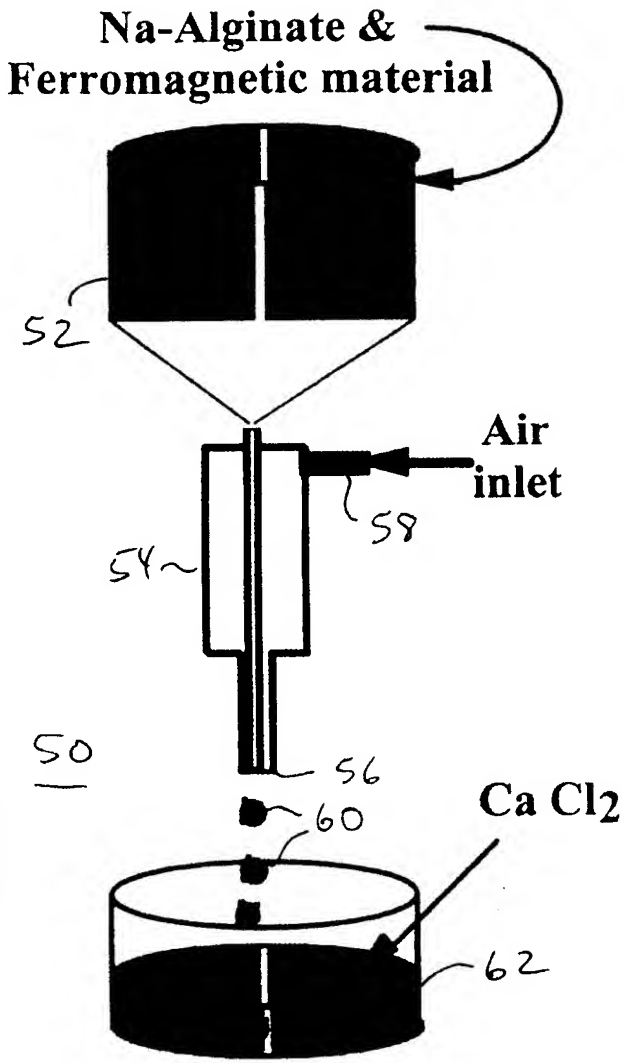

PARTICLE PRODUCTION

Pressurized Vessel

1.5% sodium alginate and 95% water are mixed with ferromagnetic material and an active substance.

Air Flow

Air flows down to tip of needle thereby shearing off a bead of desired size.

$CaCl_2$ Bath

Bivalent Ca^{2+} exchanges in for 2 Na^{+} ions thus polymerizing the alginate material.

Length of time left in $CaCl_2$ bath determines extent of polymerization.

FIG. 35

Figure 1. Schematic representation of the apparatus for the extrusion of ferromagnetic particles.

Chaplen et al.
Title: METHODS FOR DETECTING BIOACTIVE COMPOUNDS
Express Mail: EL 874430344 US
Mailed: December 17, 2001
Attorney Matter No: 245-61614

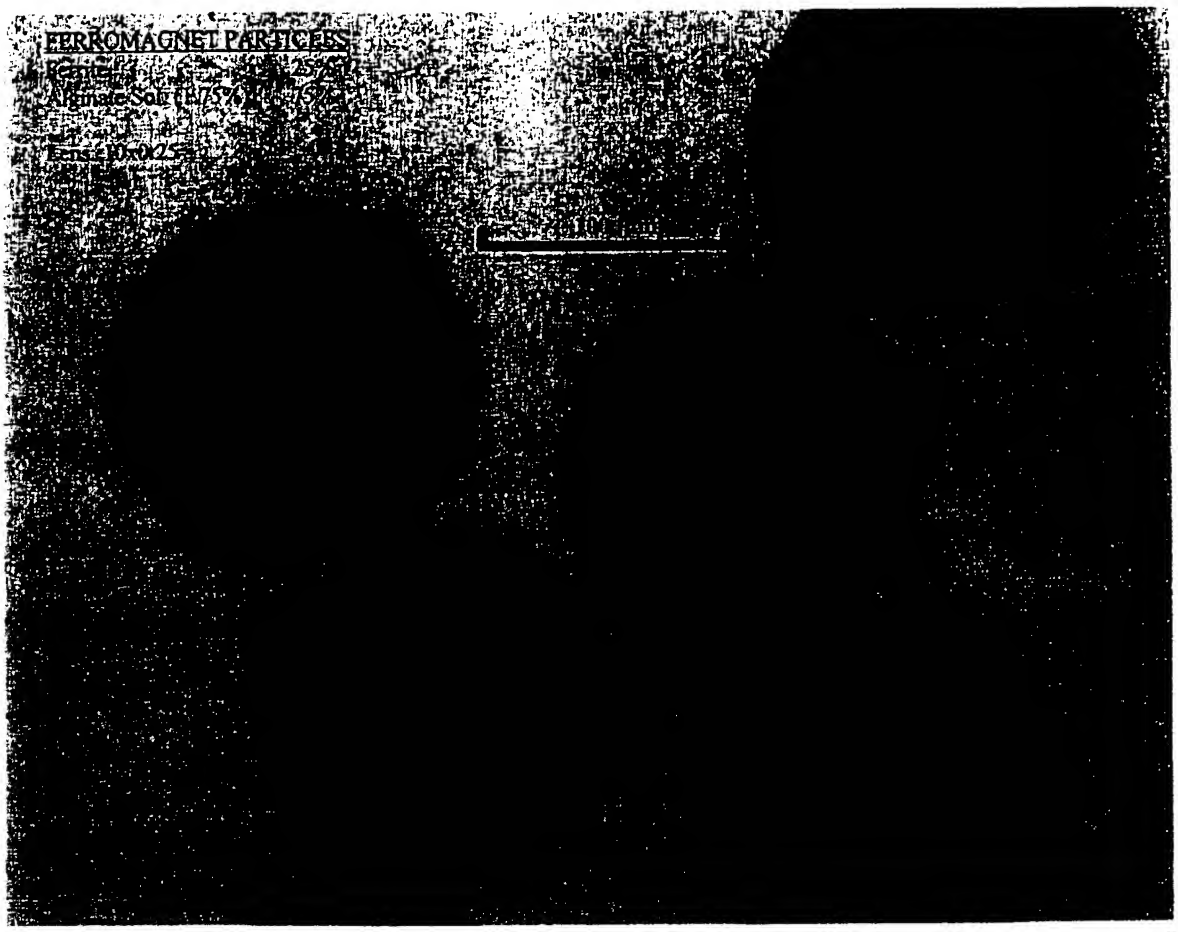

FIG. 36

Ferromagnetic micro-ball particles (dp ≈ 150 μm) produced in apparatus shown in Figure 35 (ferrite content 25%, alginate solution 75%).

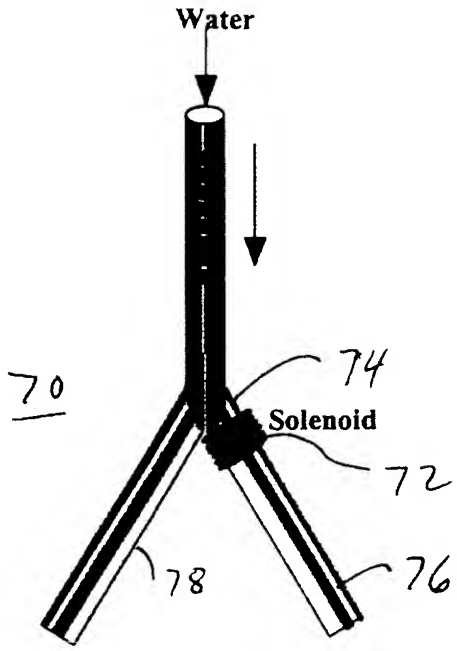

FIG. 37A

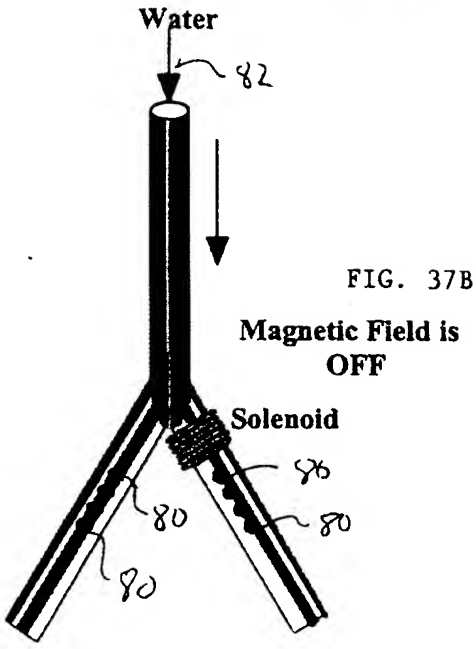

FIG. 37B

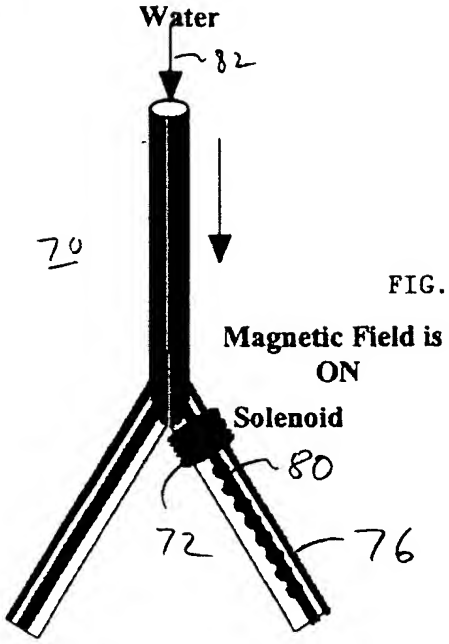

FIG. 37C

Figure 3. Schematic representation of the construction and operation of the magnetic gate.

FIG. 38A

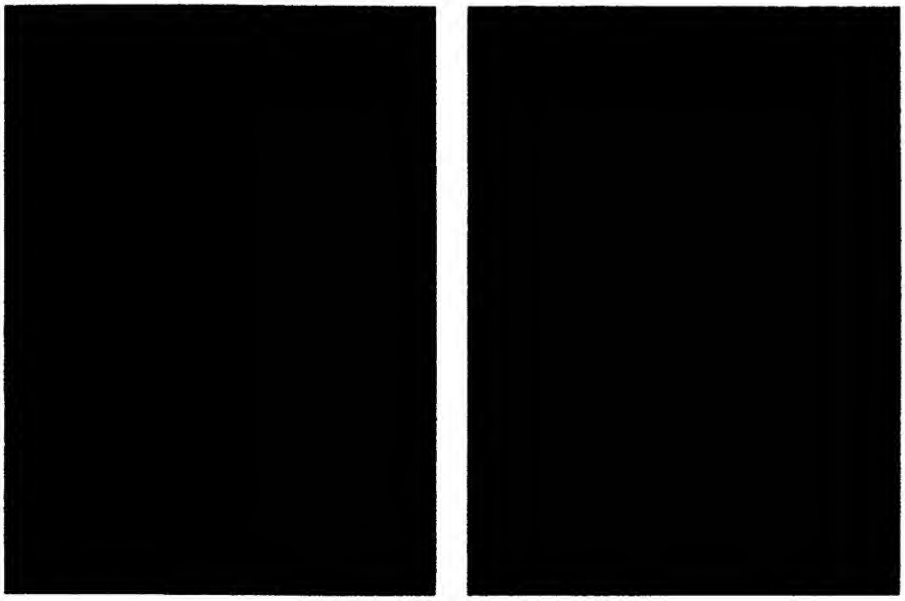

a) b)

FIG. 38B

Micrograph of the mask: a) round coil; and b) square coil.

FIG. 39

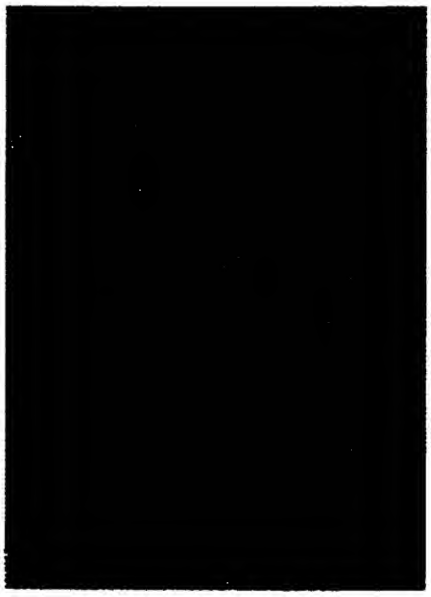

Micrograph of a 5 micron high coil made by electroforming into a lithographic mold.

FIG.40A

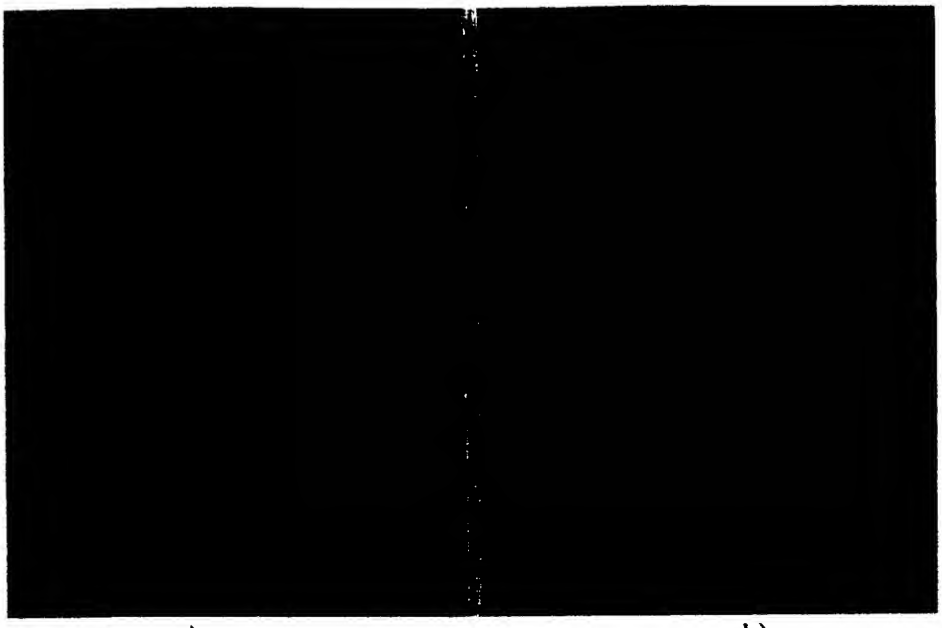

FIG. 40B

a) b)

Micrograph of the one-way micro-ball-valve: a) orifice; and b) catch plate.

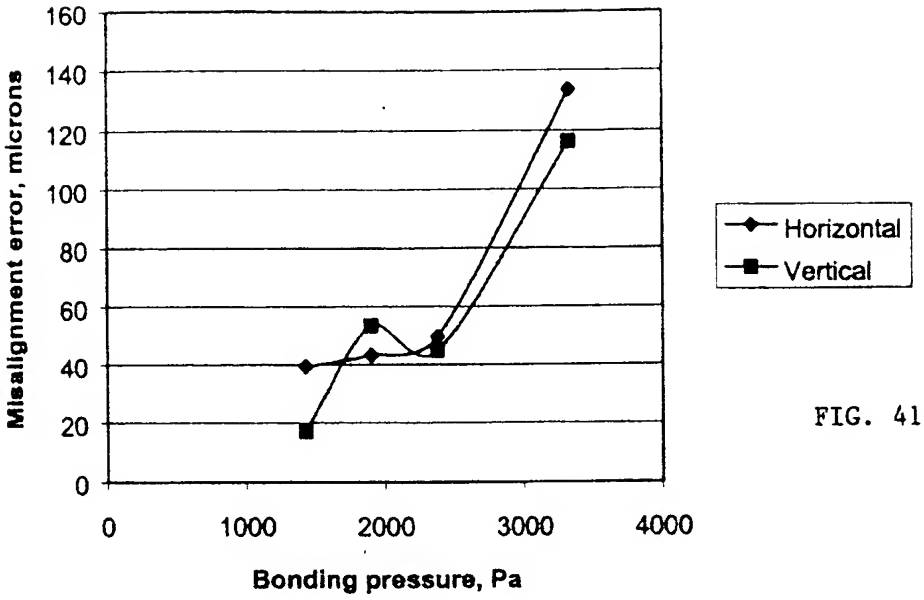

FIG. 41

Results showing effect of bonding pressure on misalignment error.

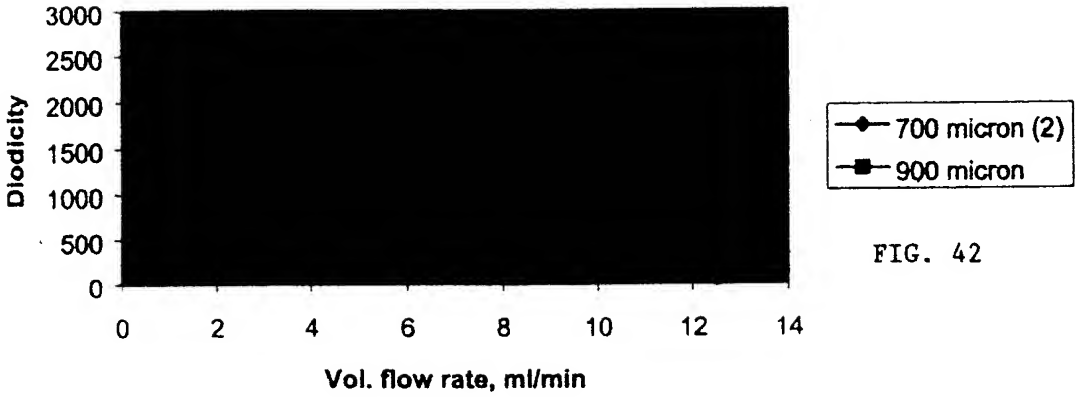

FIG. 42

Diodicity results for the last three micro-ball-valves.

Sandwich Top View with 1/16 Ports

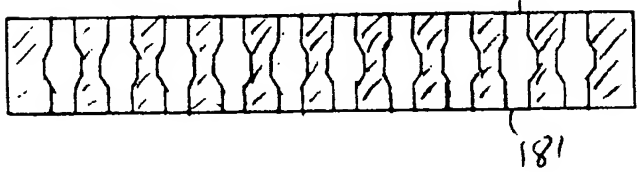

FIG. 43A

Layers Top View

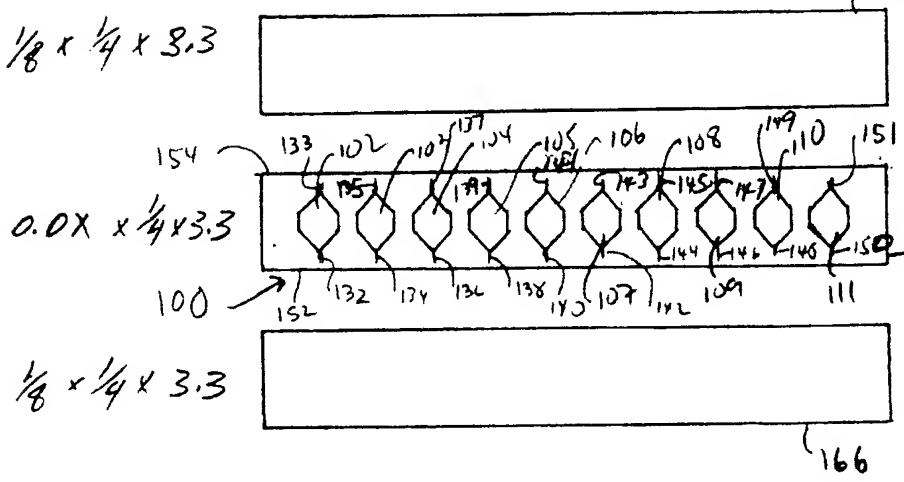

FIG. 43B

FIG. 43C

FIG. 43D

Sandwich Side View

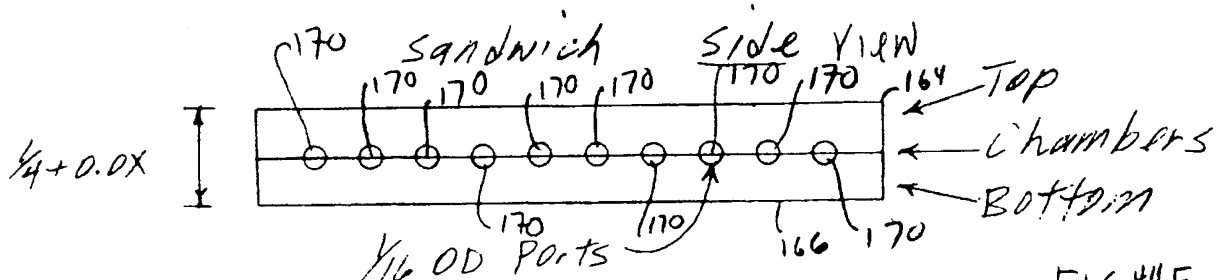

FIG. 44E

BEST AVAILABLE COPY